Steady state population balance modelling of precipitation processes: nucleation, growth and size-dependent agglomeration

Cristian Camilo Ruiz Vasquez, Noureddine Lebaz, Isabelle Ramière, Sophie Lalleman, Denis Mangin, Murielle Bertrand

Steady state population balance modelling of precipitation processes: nucleation, growth and size-dependent agglomeration

Cristian Camilo Ruiz Vasquez[1,2,*], Noureddine Lebaz[2], Isabelle Ramière[3], Sophie Lalleman[1], Denis Mangin[2], Murielle Bertrand[1],

[1] CEA, DES, ISEC, DEN, DMRC, Université Montpellier, Marcoule, France

[2] Univ Lyon, Université Claude Bernard Lyon 1, CNRS, LAGEPP UMR 5007, 43 boulevard du 11 novembre 1918, F-69100, Villeurbanne, France

[3] CEA, DEN, DEC, SESC, F- 13108 Saint-Paul Lez Durance, France

Abstract

In this work a numerical methodology to solve the steady state Population Balance Equation (PBE) is developed. Three crystallisation mechanisms are included, namely: nucleation, size-independent growth and size-dependent loose agglomeration. The numerical method is based on the discretisation of the crystal size as distributed variable. In order to describe the loose agglomeration, the numerical methodology solves two PBE: one including the nucleation and growth mechanisms and one accounting for the agglomeration process. From the first PBE, liquid phase composition, supersaturation, developed crystal surface and Crystallite Size Distribution (CSD) are obtained. Similarly, the second PBE leads to the Agglomerate Size Distribution (ASD). The study of the size-dependant agglomeration kernel induces an additional numerical difficulty due to the dependency of both PBE and agglomeration kernel on the particle size. An accelerated fixed point algorithm based on the crossed secant method is adapted to overcome the difficulty and accurately solve the agglomeration PBE. The oxalic precipitation of uranium is simulated using this numerical methodology. First, the experimental results of a reference case are compared with the numerical predictions in terms of particle size distribution, mean size, mass fraction and moments. Then, the operating conditions are varied in order to test the algorithm robustness and performances. In all cases, the crossed secant method ensures the size-dependent agglomeration PBE solution and properly predicts the ASD. The developed numerical methodology predicts the mean particle size under the experimental uncertainty in a reasonable computation time and number of iterations.

Keywords: A1. Population balance, A2. Steady state, A1. Size-dependent agglomeration, A2. Oxalic precipitation, A1. Fixed point algorithm, A1. Convergence acceleration.

[*] Corresponding author. Address: LAGEPP, Université Claude Bernard Lyon 1, bât 308G ESCPE-Lyon, 43 bd du 11 Novembre 1918, Villeurbanne 69622 France. Email address: ccrvas@gmail.com (Camilo RUIZ)

1. Introduction

The particle size distribution (PSD) is known as one of the main design specifications and process constraints in the industrial precipitation operations [1]. Indeed, the PSD obtained in the precipitation step defines the nature of the downstream unit operations (filtration, drying, calcination), the geometry of the associated apparatus and the performance of the whole solid treatment processes. Since the last century, the Population Balance Equation (PBE) has demonstrated to be an efficient numerical tool for the PSD prediction. The PBE, in its general form, is a partial differential equation (PDE) for which analytical solutions exist for a reduced number of cases only. Practically, numerical methods are commonly used for the solution of this equation. Despite the fact that different PBE numerical solution strategies are reported in the literature in the two last decades [1]–[4], efforts are still made for the development of efficient and accurate numerical formulations with reduced computational times. These aspects are ubiquitous for the elaboration of digital twins or the synthesis of real-time soft sensors for process control purposes for instance [5]. From a purely mathematical point of view, the difficulty to solve the PBE arises from:

- The different crystallization mechanisms accounted for: The complexity of the system of equations increases with the number of processes modifying the PSD.
- The form of the kinetic equations describing the crystallization mechanisms: in most cases, the relationship between the supersaturation and CSD are described by highly nonlinear equations (e.g. exponential function).
- The nature of the crystallization mechanisms: crystal growth and agglomeration can be size-dependent or independent. This condition defines whether the kinetics equations include or not the crystal size as input and output information simultaneously.

The general form of the steady state PBE in the case of a mixed suspension, mixed product removal (MSMPR) reactor when the crystal size is taken as a unique internal variable is given as [6]:

$$\frac{\partial(Gn(L))}{\partial L} + D(L) - B(L) + \sum_{i=1}^{M} \frac{F_i n_i(L)}{V} = 0 \qquad (1)$$

where G is the crystals growth rate (m.s^{-1}) , L is the crystal size (m), n_i is the number-based density function (m^{-4}) associated to the volume-based flowrate F_i (m^3.s^{-1}), n is the number-based density function (m^{-4}) of the particles inside the stirred tank, V is the total volume of the suspension in the reactor (disperse and continuous phases) (m^3), M is the total number of streams, and $B(L)$ and $D(L)$ are the birth and death terms respectively, related to the appearance and disappearance of particles in the system (through nucleation, aggregation and breakage mechanisms). Hereafter, the PSD dependence over the size will be obviated in order to simplify equations formulation ($n = n(L)$).

The precipitation concerned in this work is described by three crystallization elementary mechanisms: nucleation, crystal growth and loose agglomeration. The last one makes possible the simulation of the MSMPR by the solution of two PBE sequentially: the first one accounts for the nucleation and growth phenomena and the second one is dedicated to crystals agglomeration [7], [8]. In the scope of this work,

the crystal growth is considered as size-independent, whereas the agglomeration is defined as orthokinetic and size-dependent. Lallemand et al. (2012) described this agglomeration process by a shear-induced agglomeration kernel [7]:

$$\beta = K_a\,(L + \lambda)^3 \tag{2}$$

where β represents the agglomeration kernel ($m^3.s^{-1}$), L and λ refer to the particle size of the mother particles (m) and K_a a constant defined by thermodynamics and operating conditions.

The study of a size-dependent agglomeration kernel in the context of a MSMPR crystallizer introduces an additional dependency between the input and output variables concerned in the PBE: the agglomeration rate depends on the size of the mother particles (Equation (2)) which is itself defined by the solution of the PBE (Equation (1)). The PBE to be solved becomes even more nonlinear. For this reason, the numerical studies related to the orthokinetic agglomeration usually obviate the size dependency in the agglomeration kernel [9]–[11]. Additionally, the PBE at the steady state to directly simulate a continuous process is rarely addressed in the literature so far [12]. When treated, the kinetics of the crystallization mechanisms are often simplified in order to achieve acceptable computing times.

A numerical method to predict the size distribution of a shear-controlled flocculation process was first proposed by Koh et al. (1987) [13]. The authors developed a discretization method including only 21 geometrically distributed nodes. An orthokinetic agglomeration kernel varying with the size of the mother particles is considered but the PBE is formulated to be time-dependent. Later, Balakin et al. (2009) investigated the solution of the population balance equation including nucleation, growth, agglomeration and breakage in the context of hydrates formation within the hydrodynamic conditions determined by the recirculating system with a turbulent slurry pipe flow [14]. An orthokinetic agglomeration kernel is included in the model, however it was simplified to be independent of the particle size. The PBE is solved by tracking the time evolution of the first four moments of the PSD. It is worth noticing that, when using this specific solution methodology, a reconstruction method is necessary in order to compute the entire PSD from a reduced number of its moments [15].

Wang et al. (2005) proposed a quadrature method of moments coupled with Computational Fluid Dynamics (CFD) simulations in order to determine the mean particle size of latex spheres undergoing a laminar Taylor–Couette flow [16]. As main result, it was possible to establish a mathematical expression describing the relationship between shear rate, initial particle size and final mean size. Again, the transient PBE is solved and a reconstruction method is needed in order to describe precisely the entire PSD.

Hollander et al. (2001) investigated the influence of the distributed shear rate on the orthokinetic agglomeration [10]. For this purpose, numerical studies and experiments were carried out at several volumes of a stirred tank. Both hydrodynamics and population balance equations are solved simultaneously using a Monte Carlo method for the PBE. The initial quantity of particles and the number of nodes in the discretization scheme remain a drawback to this method in terms of computational efforts. In a second work, Hollander et al. (2001) proposed a numerical study on the coupling of

hydrodynamics and orthokinetic agglomeration [11]. Two flow patterns are studied: a turbulent channel flow and a stirred tank. Initially, a Monte Carlo-based simulation was introduced to integrate local population balances within time. However, when the simulation of a stirred tank is treated, an analytical solution based on a size-independent agglomeration kernel was preferred. The authors described the methodology as a promising alternative to reduce the computing time, however the mathematical expression of both hydrodynamics and population balance equations are simplified in order to limit the computational time.

More recently, Ochi et al. (2021) investigated the agglomeration process of polystyrene particles in a stirred tank and solved the related transient PBE [9]. Since their work is focused on establishing a relationship between the shear history and the local residence time of the particles, only two sizes of particles were considered in the suspension by simplifying the bimodal distribution. As a perspective, the authors underline the need of developing a PBE solution algorithm considering not only the mean particle size but the entire PSD.

At a more local scale, the recent works of Frungieri et al. (2020, 2021) are focused on the shear-induced aggregation/breakage of dilute colloidal suspensions [17], [18]. These pure numerical studies are based on a mixed stochastic (Monte Carlo) and deterministic (Discrete Element Method) approaches to investigate aggregation/breakage kinetics and cluster structure. Although such studies are important to bring preliminary information on the dynamic evolution of the PSD, they lack experimental validation at large scale and are known to be numerically expensive.

Even if the orthokinetic agglomeration is a well-known phenomenon, the solution of the PBE including a size-dependent agglomeration remains challenging. The computational resources required to solve the mathematical problem defined by coupling mass balances and size-dependent PBE still remain restrictive in the development of efficient modelling strategies. Furthermore, to the best of our knowledge, no attempt to solve the steady state PBE including a size-dependent agglomeration kernel is reported in literature.

As an additional constraint to the PBE solution methods, the crystallization phenomena and the hydrodynamics prevailing in the precipitator are closely related. Indeed, the micro and macro mixing patterns define the concentration gradients and the local supersaturation, the mass transfer between the solution and the crystals and the collision and fragmentation rates of the particles. In order to model the crystallization operations and simulate the outlet PSD, the numerical solution methods of the PBE need to be suitable for coupling with any hydrodynamic model or with Computational Fluid Dynamics (CFD).

The purpose of this work is to develop a methodology for the prediction of the PSD obtained in a steady state MSMPR undergoing nucleation, growth and loose agglomeration. Its novelty relies on the solution of the steady state PBE in the case of a size-dependent agglomeration process. Additionally, the

developed methodology needs to be numerically efficient to guarantee a robust numerical solution of the PBE, to enable the PBE to be implemented in a multi-compartmental model representing the hydrodynamics of a real reactor.

In a previous work [8], a methodology to solve the steady state PBE including nucleation, growth and loose size-independent agglomeration was introduced and validated. The agglomeration PBE was solved by an accelerated fixed-point method. The validation of the numerical approach was carried out considering the precipitation of neodymium oxalate. In such case, the agglomeration process was described by a constant agglomeration kernel [7]. In the present work, the same methodology is extended to the simulation of a size-dependent agglomeration process (equation (2)). The case study is defined by the oxalic precipitation of uranium in a MSMPR following the reaction:

$$U(NO_3)_4 + 2H_2C_2O_4 \xrightarrow{H_2O} U(C_2O_4)_2, 6H_2O + 4HNO_3 \quad (3)$$

In the nuclear industry, this reaction is widely used as the main conversion and purification stage leading to the production of an actinide rich powder from a multicomponent solution. The characteristic time of the reaction is fast enough in comparison to the crystallization time scale, the influence of the reaction kinetics on the whole process is then neglected. In this case the agglomeration kernel is size-dependant, which challenges the numerical method and requires modifications specifically in the convergence criterion.

The structure of this paper is as follows: in Section 2, the numerical methodology for solving the PBE is summed up, describing the accelerated fixed point algorithm to solve the size-dependent agglomeration PBE at steady state. An appropriate convergence criterion is introduced in order to determine accurately the convergence in terms of the PSD. In Section 3, simulation predictions are compared to experimental results, first by comparison to a reference case and then against a range of experimental data by modifying the initial concentration of reactants and the stirring rate. Finally, some concluding remarks and perspectives are pointed out.

2. Modelling strategy

Uranium oxalate crystals have been identified as loose (open) agglomerates according to microscopic observations: the crystal surface area is the same at any stage of the agglomeration process [7]. Thus, the surface available to mass transfer between the liquid and the solid phases is defined by the crystallites (monoparticles), independently of the agglomeration process. Consequently, the agglomeration process does not modify the concentrations of the liquid phase, but only the particles shape and volume [7]. Thus, only the nucleation and growth phenomena contribute to the mass transfer between the solid and the liquid phases. Considering this, the steady state PBE (Equation (1)) solution is performed by describing the whole precipitation process through two distinct PBEs solved successively. The first one accounts for nucleation and growth mechanisms, and the second one considers the crystallites agglomeration only, using the CSD obtained as a result of the first PBE.

The precipitation concerned in this work takes place in a MSMPR operating at the steady state. Several inlet flows $(F_i)_{i=1}^{M-1}$ are considered and one single exit flow (F_M). The mean residence time is thus defined as $\tau = \frac{V}{F_M}$ with the outgoing flow rate $F_M = \sum_{i=1}^{M-1} F_i$. The equation (1) including all the crystallization mechanisms (nucleation, growth and agglomeration) can be expressed as a combination of two different PBEs as explained earlier. The first one described by Equation (4) accounts for the nucleation and size-independent growth phenomena and determines the total developed surface of the crystals.

$$G\frac{dn_{out,1}}{dL} + \frac{n_{out,1}}{\tau} - \frac{\frac{\sum_{i=1}^{M-1} F_i\, n_i}{F_M}}{\tau} = r_N \cdot \delta(L - L^*) \qquad (4)$$

where δ is the Dirac delta function, L^* the nucleus size (m), r_N ($m^{-3}.s^{-1}$) the nucleation rate, and $n_{out,1}$ the number-based density associated to the output stream (CSD).

Then, the second PBE includes the agglomeration process only and determines the final PSD, as given in Equation (5):

$$\frac{n_{out,2} - \frac{\sum_{i=1}^{M-1} F_i\, n_i}{F_M}}{\tau} = \frac{L^2}{2}\int_0^L \frac{\beta\left((L^3-\lambda^3)^{1/3}, \lambda\right) n_{out,2}\left((L^3-\lambda^3)^{1/3}\right) n_{out,2}(\lambda)\, d\lambda}{(L^3-\lambda^3)^{2/3}} - n_{out,2}(L)\int_0^\infty \beta(L,\lambda)\, n_{out,2}(\lambda) d\lambda \qquad (5)$$

where β is the agglomeration kernel ($m^3.s^{-1}$) and $n_{out,2}$ represents the agglomerates size distribution.

The simulation of the entire precipitation operation is achieved by solving both PBEs sequentially: the CSD obtained from Equation (4), called $n_{out,1}$, constitutes an input information to solve the second PBE (equation (5)). Additionally, by coupling the mass balance and nucleation-growth PBE, it is possible to predict the liquid phase composition and the crystallite size distribution. The final PSD (i.e. the agglomerates size distribution) leaving the MSMPR ($n_{out,2}$) is determined by the agglomeration PBE. Previously, a similar methodology was implemented in order to determine the neodymium oxalate size-independent agglomeration kernel [7] and to model the neodymium oxalate precipitation in a MSMPR [8].

2.1. Nucleation and growth PBE solution

Equation (4) is an ordinary differential equation which can be easily solved when the inlet population (n_i) and the nucleation and growth rates are known. In this case, it is solved simultaneously with the mass balance by a minimisation iterative gradient-based method (Sequential Quadratic Programming method). The objective function aims to converge to a limit reactant concentration in solution satisfying both the PBE and the mass balances. The stopping criterion is determined by the relative difference between the concentration calculated at two successive iterations.

2.2. Fixed-point agglomeration PBE solution

The agglomeration PBE is also solved by a discretization method. Kumar and Ramkrishna (1996) [19] formulated the agglomeration rate (right side of equation (5)) under its discretized form as:

$$r_{Ag}(L_k) = \sum_{\substack{p,q=1 \\ p\geq q}}^{p=K} \left[\left(1-\tfrac{1}{2}\delta_{p,q}\right)\eta\,\beta(L_p,L_q)\;\; N_{out,2}(L_p)N_{out,2}(L_q)\;\right] - \; N_{out,2}(L_k)\sum_{r=1}^{K}\beta(L_k,L_r)\; N_{out,2}(L_r) \qquad (6)$$

with $r_{Ag}(L_k)$ the agglomeration rate ($m^{-3}s^{-1}$) and K the number of the discretisation nodes. Under the following conditions:

$$L = \left(L_p^3 + L_q^3\right)^{1/3},\;\; L_{k-1} \leq L \leq L_{k+1} \qquad (7)$$

$$\eta = \begin{cases} \dfrac{L_{k+1}^3 - L^3}{L_{k+1}^3 - L_k^3}, & L_k \leq L \leq L_{k+1} \\ \dfrac{L^3 - L_{k-1}^3}{L_k^3 - L_{k-1}^3}, & L_{k-1} \leq L \leq L_k \end{cases} \qquad (8)$$

where $\delta_{p,q}$ is defined as the Kronecker delta function, $N_{2,out}(L_k)$ represents the total number of particles in the *k*th size range (class). The weight coefficient η ensures the conservation of two properties: number and mass after the numerical transformation from the original agglomeration PBE (equation (5)) to the discretized agglomeration PBE (equation (6)).

In the agglomeration problem, the unknown variable is defined as $N_{2,out}(L_k)_{k=1}^{K} = \boldsymbol{N}$ which refers to the vector resulting from the discretization of the number-based PSD over the particle size $(L_k)_{k=1}^{K}$. By defining the inlet population (before agglomeration process) as $\boldsymbol{N}_{in} = N_{in}(L_k)_{k=1}^{K} = \frac{\sum_{i=1}^{M-1} F_i\, N_i(L_k)_{k=1}^{K}}{F_{out}}$, equation (6) can be reformulated as a fixed point problem:

$$\boldsymbol{N} = \boldsymbol{f}(\boldsymbol{N}) = \boldsymbol{N}_{in} + \tau\, \boldsymbol{r_{Ag}}(\boldsymbol{N}) \qquad (9)$$

where the function $f(\boldsymbol{N})$ represents the agglomeration PBE under its vector form.

Fixed point problems are often solved by fixed point iterations, also called Picard iterations:

$$\boldsymbol{N}^j = \boldsymbol{f}(\boldsymbol{N}^{j-1}) = \boldsymbol{N}_{in} + \tau\, \boldsymbol{r_{Ag}}(\boldsymbol{N}^{j-1}) \qquad (10)$$

It is possible to apply an acceleration method in order to improve the convergence and robustness of the fixed point algorithm. This consists in substituting the current fixed point value ($\boldsymbol{f}(\boldsymbol{N}^{j-1})$), by an accelerated iterate [20]. In general, it is defined as a function of the previous accelerated and standard iterates [21].

The crossed secant method was previously demonstrated to be efficient enough to solve the size-independent agglomeration PBE [8]. In this case, the iterates $\boldsymbol{N}^j$ are defined as:

$$\boldsymbol{N}^j = \boldsymbol{f}(\boldsymbol{N}^{j-1}) - \frac{\left(\boldsymbol{f}(\boldsymbol{N}^{j-1}) - \boldsymbol{f}(\boldsymbol{N}^{j-2})\right)\cdot(\Delta\boldsymbol{N}^{j-1} - \Delta\boldsymbol{N}^{j-2})}{\|\Delta\boldsymbol{N}^{j-1} - \Delta\boldsymbol{N}^{j-2}\|^2}\,\Delta\boldsymbol{N}^{j-1} \qquad (11)$$

where j represents the iteration index, ||.|| the Euclidean norm and $\Delta \boldsymbol{N}^j = \boldsymbol{f}(\boldsymbol{N}^j) - \boldsymbol{N}^j$. The same method is implemented in this work to solve the size-dependent agglomeration PBE, such as in the context of the uranium precipitation.

2.3. Fixed point convergence criterion

In precipitation models, the PSD takes values close to zero in the regions corresponding to very small and large sizes. In contrast, the same PSD is commonly several orders of magnitude above near to the peak region**.** As the objective variable ($\boldsymbol{N}$) of the fixed point problem varies over several orders of magnitude (between 0 and 10^{15} in the case of the uranium oxalate), a mixed convergence criterion [22] is first proposed as in [9]:

$$\left| f_k(\boldsymbol{N}^j) - N_k^j \right| < \varepsilon_r \left| N_k^j \right| + \varepsilon_a, \ \forall k \tag{12}$$

where the index k refers to the k^{th} component of the vector. This criterion has to be evaluated before applying (or not in case of convergence) the acceleration method. The accelerated iterate will be used as input for the next iteration. In practice, it is common to represent equation (12) as a boolean:

$$\max_{(\mathbf{k})} \left(\left| f_k(\boldsymbol{N}^j) - N_k^j \right| - \varepsilon_r \left| N_k^j \right| - \varepsilon_a \right) < 0 \tag{13}$$

Through Equation (12), the fixed point convergence is reached when the fixed point residual is less than the total of the tolerances. The convergence test includes two tolerance constants: the relative tolerance ε_r and the absolute tolerance ε_a. This convergence criterion turns automatically from a relative error to an absolute error when $\left| N_k^j \right|$ becomes small enough. Hence it enables to deal in a unique criterion with high values of N components (for which the relative precision is recommended) and small values of N components (where absolute tolerance is required).

The application of Equation (12) as convergence criterion is constrained to the fact that close to convergence, the objective function ($f(\boldsymbol{N})$) does not deviate too much from the fixed point and remains reliable. In the case of the orthokinetic size-dependent kernel treated in this work, the range of validity of the objective function may be compromised especially for large particle sizes (see Section 3.1 for a detailed numerical analysis). For this reason, a stopping criterion based on the accelerated iterates is preferred:

$$\max_{(\mathbf{k})} \left(\left| N_k^{j+1} - N_k^j \right| - \varepsilon_r \left| N_k^j \right| - \varepsilon_a \right) < 0 \tag{14}$$

This stopping criterion consists in checking the convergence of the accelerated sequence and returns to Equation (13) in case of standard fixed point iteration (cf. Equation (10)).

In the case of size-dependent agglomeration, the absolute tolerance is reformulated in order to fit the variation of the agglomeration kernel over the size range:

$$\varepsilon_a = \frac{\max_{(k)}(\boldsymbol{N}_{in})\, t'}{\varepsilon'_a} \tag{15}$$

where ε'_a is a constant associated to the absolute tolerance and t' the dimensionless agglomeration time, defined by [23]:

$$t' = N_0\, \beta\, \tau \tag{16}$$

It is worth noticing that when the peak region (high values of N components) is of interest, the absolute tolerance could remain relatively high, in order to focus on the convergence of the solution in the peak region (with a relative error).

3. Results and discussion

In this section, the numerical results obtained by the methodology described in section 2 are compared to experimental measurements. For this purpose, oxalic precipitation of uranium was carried out in a stirred tank reactor provided with a heating jacket by mixing an aqueous solution of uranium nitrate with an aqueous solution of oxalic acid. Mixing was performed by a stainless-steel turbine equipped with four 45° pitched blades. The reagent concentrations in the reactor obey to the stoichiometric ratio of equation (3) and the uranium oxalate is meant to be the only compound found in the solid phase.

The nucleation rate r_N for the uranium oxalate was expressed by considering the classical nucleation theory [24]:

$$r_N = a_N\, exp\left(-\frac{E_N}{R\,T}\right)\, exp\left(-\frac{b_N}{(\ln S)^2}\right) \tag{17}$$

with T the temperature (K), R the ideal gas constant (J mol^{-1} K^{-1}), E_N the nucleation energy activation (kJ mol^{-1}), S the supersaturation ratio, a_N (m^{-3} s^{-1}) and b_N (-) are nucleation kinetic constants.

In the case of oxalic precipitation of uranium, the crystal growth rate was found to be independent of the crystal size and integration-controlled (i.e. a rapid mass transfer with respect to the integration kinetics) [24]:

$$G = a_G \exp\left(-\frac{E_G}{R\,T}\right) s \tag{18}$$

where E_G represents the growth process activation energy (kJ mol^{-1}), s the absolute supersaturation (mol m^{-3}) and a_G a growth kinetic constant (m^4 mol^{-1} s^{-1}). In contrast, the uranium oxalate agglomeration process was found to be dependent of the crystal size according to a turbulent orthokinetic-like-kernel which also depends on ionic strength, supersaturation and temperature (as in the case of neodymium oxalate [7]). Thus the agglomeration kinetics is expressed as [24]:

$$\beta = a_\beta\, I^{b_\beta}(S-1)\,\dot{\gamma}\, \exp\left(-\frac{E_\beta}{R\,T}\right)(L+\lambda)^3 \tag{19}$$

where $\dot{\gamma}$ is the shear rate (s^{-1}), E_β is the activation energy (kJ mol^{-1}), I is the ionic strength of the solution (mol m^{-3}), a_β ($\mathrm{m}^{3\mathrm{b}\beta}\ \mathrm{mol}^{-\mathrm{b}\beta}$) and b_β (-) are constants.

For a better understanding and comparison of the numerical and experimental data, the results are presented in the next section under their dimensionless form:

- The mean agglomerates size is systematically divided by the highest value of this variable (Experiment 5 in Table 1):

$$\bar{d}_{43} = \frac{d_{43}}{d_{43,max}} \tag{20}$$

- Similarly, the mean crystallites size is systematically divided by the crystallites size exhibited by the Experiment 5 in Table 1.
- The crystal size range is reduced to [0, 1] by defining a dimensionless length:

$$\bar{\boldsymbol{L}} = \frac{\boldsymbol{L}}{L_{max}} \tag{21}$$

  where L_{max} (m) corresponds to the maximum in the crystal size scale;

- The PSDs are normalized as follows:

$$\bar{N} = \frac{\boldsymbol{N}}{N_{max}} \tag{22}$$

- Finally, the moments of any distribution are presented as standard moments:

$$\bar{\mu}_l = \frac{\mu_l}{\mu_2^{l/2}} \tag{23}$$

3.1. Numerical analysis

In this section, the numerical behaviour of the agglomeration solution algorithm is examined. To this end, the nature of the target variable needs to be considered. The seek variable of the fixed point iterations is the PSD obtained during an orthokinetic agglomeration process, referred to as $\boldsymbol{N}$.

To illustrate the performance of the acceleration algorithm and the limit of the standard fixed point stopping criterion (see Equation (12)) for a size-dependent kernel, the experiment 1 of Table 2 is considered. Figure 1 displays the standard iterate and the accelerated iterate of two successive iterations (49th and 50th). It is worth noticing that the PSD obtained by the crossed secant exhibits the same shape over two iterations. In this figure, the standard and the accelerated iterates ($f(\boldsymbol{N}^j)$ and $\boldsymbol{N}^{j+1}$ respectively) are normalized based on the maximum value of the last accelerated iterate (namely $\boldsymbol{N}^j$) in order to compare the three PSDs between two iterations. Further, the same conclusion is made when the accelerated iterates are compared between the 40th and 60th iterations. However, it is not the case for the fixed point iterate that seems to predict artefacts for large particles. From this iteration, the PSD obtained oscillates between two states: the first corresponds to the acceleration method prediction while the second one is obtained by the numerical integration of the agglomeration PBE from the accelerated input.

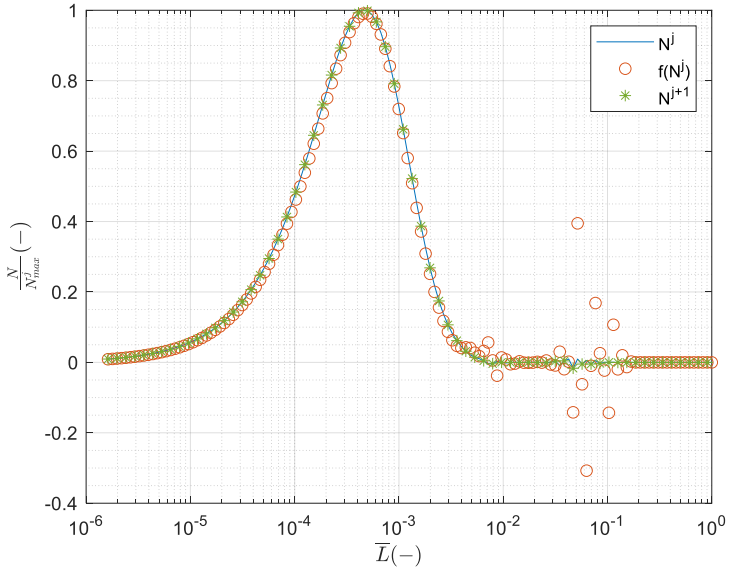

Figure 1. Dimensionless PSD comparison between the standard (red) and accelerated (green) iterates (between 49th and 50th iterations).

Agglomeration process is the result of several types of interaction between the crystallites. At least three different forces are identified in the literature as responsible of collision during this process: Brownian coagulation associated with particles under a size of 1 µm, shear-induced orthokinetic agglomeration typically describing the agglomerations of particles between 1 µm and 40 µm and finally sedimentation occurring when the size range exceeds 40 µm [25]–[27].

In the case of the PSD obtained during the uranium precipitation, the particle size varies over 4 orders of magnitude. It is then possible to say that the balance between the different collision forces varies between the particles at the beginning and the end of the size range. Consequently, the agglomeration kernel proposed to simulate the uranium oxalic precipitation fits better the size region near to the peak than the larger sizes. Indeed, Mersmann (2001) established the range of validity of the shear-induced agglomeration kernel (equation (2)) between 0 and 100 µm [28], the flat region in Figure 1 is widely over this value. This behaviour is observed in Figure 2 which depicts the agglomeration kinetics in comparison to the PSD for the same iteration.

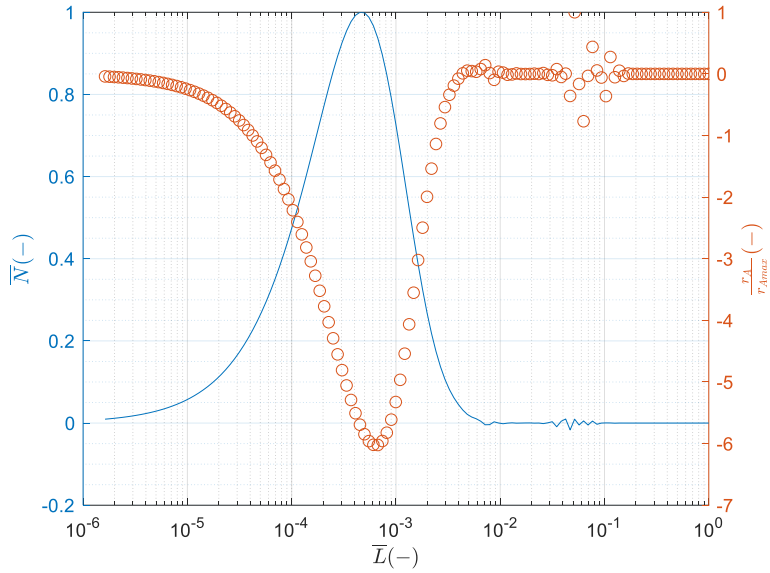

Figure 2 . Agglomeration kinetics (right axis) and PSD (left axis) over the dimensionless particle size at iteration 50 of the agglomeration PBE solving process (Experiment 1 in Table 1).

The perturbations observed in the size range [10^{-2}, 1] in Figure 1 are directly caused by the behaviour of the agglomeration kinetics (equation (6)) and can be explained by:

- The propagation of the numerical error associated to the agglomeration PBE numerical integration,
- The agglomeration kernel: since the agglomeration kernel was deduced from experimental results (typically between 0,5 and 200 µm), the accuracy to predict the number of particles in a size range in which no or very few particles were measured (flat regions) is very low,
- The order of magnitude of the size range: since the agglomeration kernel includes the particle size to the power of three, small errors in the agglomeration kinetics are amplified when the PSD is considered.

In conclusion, the perturbations observed in the PSDs are induced by the modelling methodology and do not correspond to any physicochemical phenomenon occurring during the agglomeration process. In the other hand, the shape of the PSD obtained by the crossed secant method is consistent with the monomodal distribution expected as the outgoing PSD in the uranium precipitation. In consequence, the stopping criterion based on the accelerate iterates is preferred to formulate the convergence criterion, see equation (14).

The evolution of this convergence criterion over the iterations is shown in Figure 3 ($\varepsilon'_a = 10^{-4}$ and $\varepsilon_r = 10^{-3}$). Similarly, the evolution of the volume-based mean diameter is presented in Figure 4. In both cases, it is possible to observe the algorithm evolution: the convergence criterion drops to zero while the mean crystal size oscillates until stabilisation.

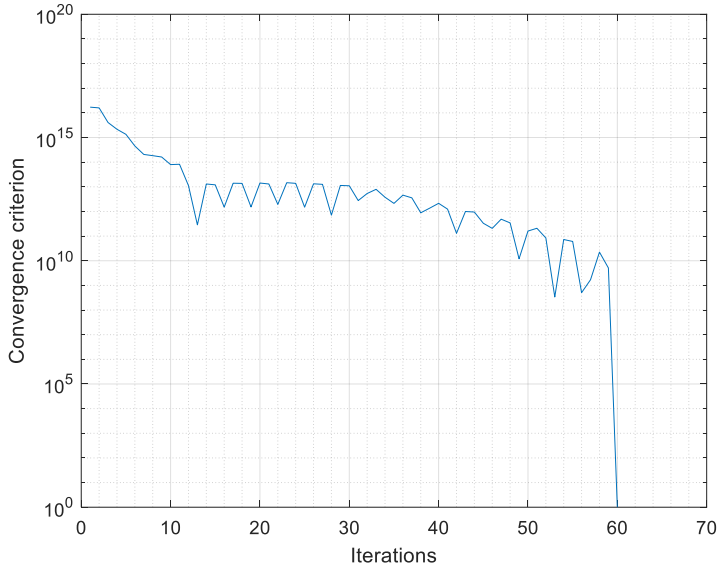

Figure 3. Evolution of the convergence criterion on the accelerated sequence in the case of a MSMPR modelling including nucleation, size-independent growth and loose agglomeration with crossed secant algorithm.

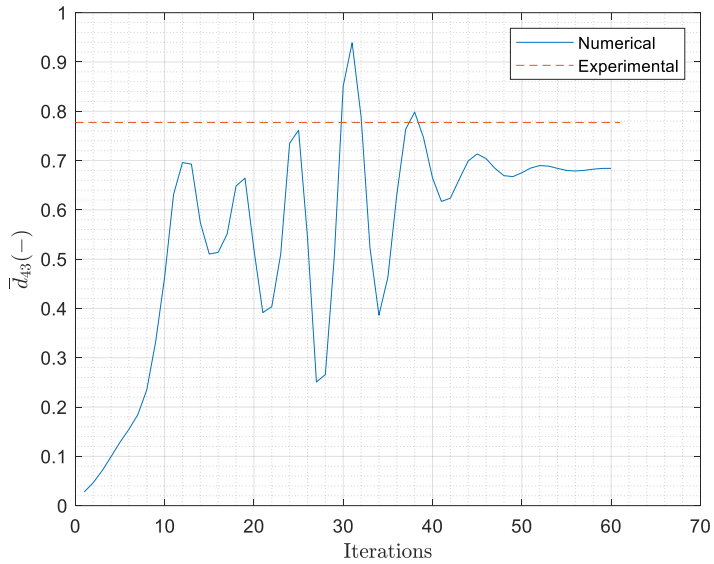

Figure 4. Mean particle size evolution in the case of a MSMPR modelling including nucleation, size-independent growth and loose agglomeration with accelerated fixed point algorithm.

In both Figure 3 and Figure 4, it is worth noticing that the fixed point iterates can be seen as pseudo-transient solutions (pseudo-time steps) before reaching the steady state. Further, the convergence criterion proposed here stops the fixed point iterations when the mean size becomes stable over the iterations. Even if the convergence of the standard fixed point cannot be obtained through the given orthokinetic kernel which seems not valid at high crystal size, the application of the crossed secant method associated to the convergence criterion proposed in Equation (32) correctly drives the algorithm to convergence. This confirms the robustness of the proposed algorithm, since the crossed secant method makes up for the shortcomings of modelling.

3.2. Numerical and experimental results

In this section the results obtained by the numerical methodology presented in section 2 are compared to experimental results obtained in a stirred tank reactor operating at steady state. First, equation (4) is solved to obtain crystallites size distribution and supersaturation. Afterwards, Equation (5) determines loose agglomerates size distribution. All the simulations are carried out on an Intel Core i7 machine (1.90 GHz/ 2.11 GHz) with 32 Go of RAM, the relative tolerance (ε_r) is fixed to 10^{-3} (0.1%) while the constant in the absolute tolerance is $\varepsilon'_a = 10^{-4}$. Finally, the discretization grid contains 1500 logarithmically distributed points and the initial vector for the fixed point algorithm solving the agglomeration PBE is set to zero.

3.2.1. Reference case

First, the developed methodology is tested against a reference experiment (Experiment 8 in Table 1)**~~Erreur ! Source du renvoi introuvable.~~**. Figure 5 presents a comparison between the numerical and the experimental results in terms of mean crystal size (a) (obtained as the ratio between the 3rd and 4th moments), mass fraction (b) and moments (c) at convergence.

The crystal mean size is predicted with a relative error of 13%. Concerning the moments prediction, the highest relative error takes a value around 5% (0th order moment). In contrast, a broader difference is observed when the entire PSD is examined. The gap between the simulated and the experimental CSD arises from the uncertainty associated to the crystallization kinetics. Firstly, nucleation kinetics typically predicts the quantity of elementary crystals over one order of magnitude. Secondly, the methodology employed to determine the constants associated to the uranium oxalate agglomeration kernel includes the solution of the PBE by the moments method [7]. Such numerical treatment ensures a precise calculation of the moments but generates errors in the PSD prediction due to the lack of information about the entire distribution. The difference between the numerical and experimental agglomerates size is then explained by the inherent gap between the two methods to solve the PBE: the moments method, used to determine the constants $\boldsymbol{a_\beta}$, $\boldsymbol{b_\beta}$ and $\boldsymbol{E_\beta}$ in equation (19) by Lalleman et al. (2012) and the discretization method used to determine the PSC in this paper.

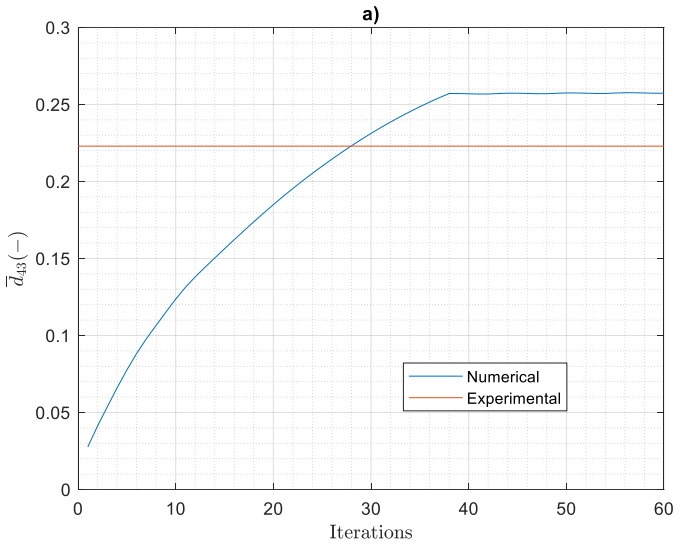
a)
0.3
0.25
0.2
0.15
0.1
0.05
0
$\overline{d}_{43}(-)$
0
10
20
30
40
50
60
Iterations
Numerical
Experimental

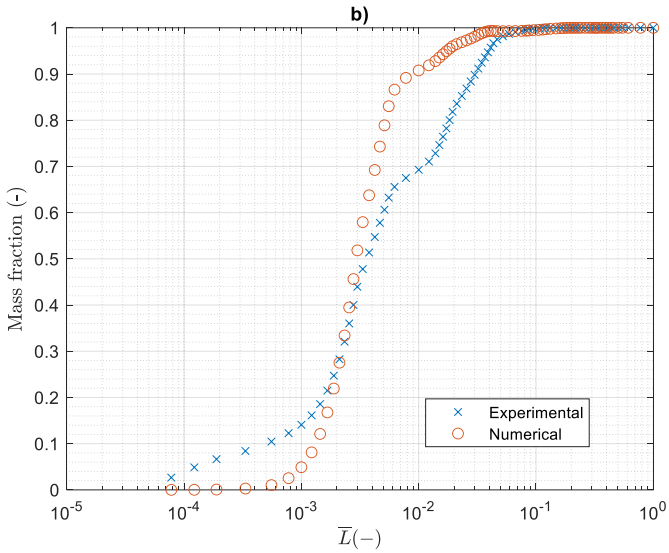
b)
1
0.9
0.8
0.7
0.6
0.5
0.4
0.3
0.2
0.1
0
Mass fraction (-)
10^{-5}
10^{-4}
10^{-3}
10^{-2}
10^{-1}
10^{0}
$\overline{L}(-)$
Experimental
Numerical

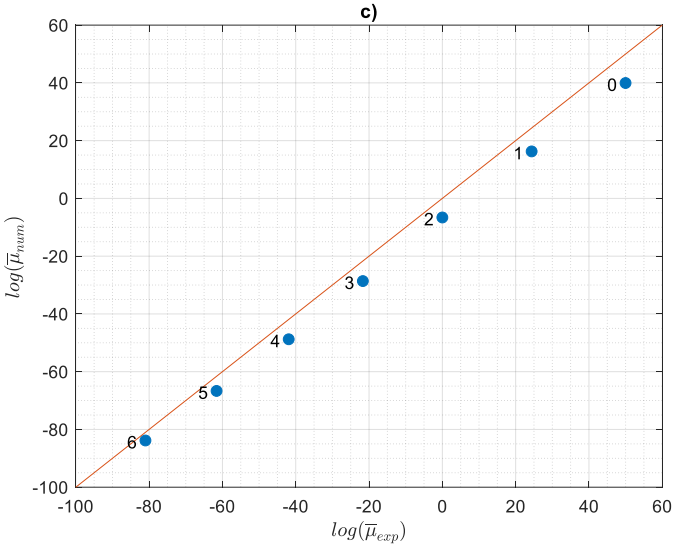

Figure 5. Experimental and simulation results in the case of a MSMPR including nucleation, size-independent growth and loose size-dependent agglomeration: a) Mean crystal size prediction over the number of iterations b) Mass-based CSD and c) CSD moments at convergence (iteration 36).

3.2.2. Sensitivity analysis

In order to study the algorithm robustness, its response is tested by varying three of the operating conditions: the residence time, the shear rate via the stirring rate and the total uranium concentration via the inlet stream concentration. The experimental results and the numerical predictions in terms of mean particle size and elementary crystallites size are presented in Table 1.

Table 1 Experimental conditions (Uranium concentration in the inlet flow, residence time and shear rate) and mean particle size for the simulation of a continuous stirred crystallizer (MSMPR) including nucleation, size-independent growth and loose agglomeration.

Experiment	$[U]/[U]_{max}$ (-)	Residence time (s)	$\dot{\gamma}$ (s^{-1})	Simulated crystallites $\bar{d}_{43}$(-)	Experimental $\bar{d}_{43}$ (-)	Simulated $\bar{d}_{43}$ (-)
1	0.61	60	349	0.8	0.78	0.68
2	1.02	121	349	1.15	0.65	0.58
3	1.03	120	349	1.2	0.75	0.59
4	0.19	119	349	1.2	0.55	0.61
5	1.00	60	349	1	1	0.85
6	0.65	60	124	0.8	0.26	0.22
7	0.61	60	349	0.8	0.76	0.68
8	0.61	60	124	0.8	0.22	0.25
9	0.61	60	642	0.8	0.75	0.81

Experiments (1,7) and (2,3), performed under the same conditions, provide indications dealing with the experimental uncertainty. Experimental and numerical volume-based mean sizes (d_{43}) obtained for the experiments described in Table 1 are plotted in Figure 6. In all cases, the numerical methodology predicts the particle mean size under the experimental uncertainty (dotted lines). The crystallite and final agglomerate sizes are dimensionless, expressed with respect to the largest size of crystallites and that of agglomerates, respectively.

In crystallization, a higher residence time is generally associated with larger particles since the crystals are longer in contact with the solution and the mass transfer can operate. If experiments 2 and 5 are compared, this trend is well observed with the crystallite size, which increases when the residence time increases from 60s to 121s. However, it is interesting to notice that the mean size of the agglomerates varies on the opposite direction and that the simulation is able to describe this behaviour.

Experiments 5, 6, 7, 8 and 9 exhibit the same crystallites mean size. It is then possible to say that the agglomeration process is the only mechanism responsible for differentiating the final mean particle size in these cases. Additionally, experiments 7, 8 and 9 present the same uranium concentration and residence time but different shear rates, meanwhile experiments 5, 6 and 7 undergo the same shear rate but different concentrations. The same variation in terms of the operating conditions has different consequences on the nucleation, growth and agglomeration kinetics. The developed methodology depicts at the same time the evolution of the target variables (PSD and composition) and the intermediate physicochemical properties (supersaturation, crystallization kinetics).

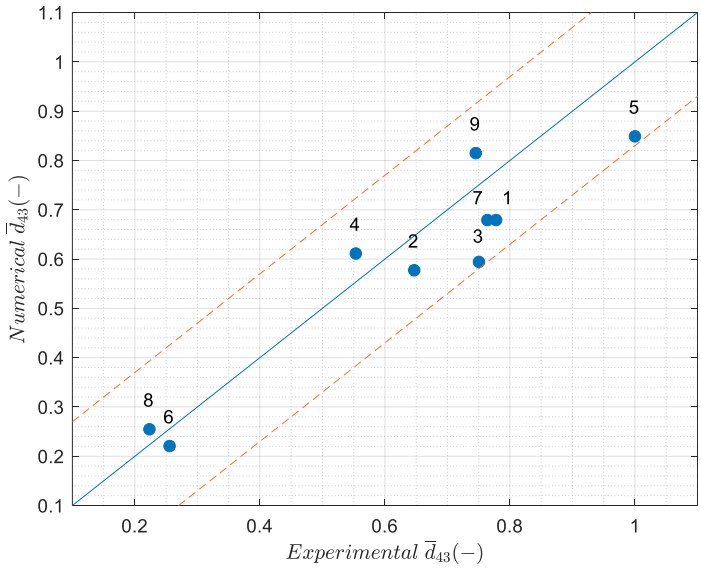

Figure 6. Comparison between experimental and simulated mean crystal sizes for the conditions reported in ~~**Erreur ! Source du renvoi introuvable.**~~Table 1.

Experiments 4, 1 and 2 are carried out at different values of the feeding uranium concentration. The corresponding mean agglomerate sizes are presented in Figure 7. In crystallization, a higher concentration implies a higher supersaturation and enhances crystallization phenomena rates. It is then

common to obtain larger particles when the concentration is raised. Meanwhile, the crystal size does not depend solely on the uranium concentration, both the residence time and the supersaturation modify the balance between the nucleation, growth and agglomeration phenomena. For this reason, the particle size may increase (experiments 4 and 1) or decrease (experiments 1 and 2) with the uranium concentration. In both cases and even when the evolution of the PSD follows an *a priori* non-intuitive behaviour, the numerical methodology describes correctly the direction and proportion of the mean size variation. This again confirms the robustness of the proposed numerical strategy.

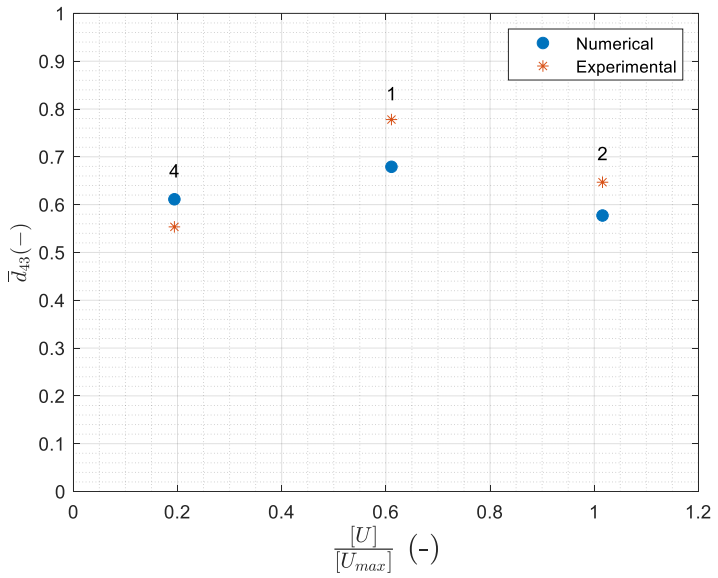

Figure 7. Numerical and experimental mean crystal size evolution over the inlet uranium concentration in the case of a MSMPR including nucleation, size-independent growth and loose size-dependent agglomeration.

Similarly, Figure 8 focuses on the influence of the shear rate over the mean crystal size. It concerns the experiments 7, 8 and 9 in Table 1. It is possible to say that the mean particle size increases with the shear rate. Whether the shear rate increases from 124 to 349 or 642, the mean particle size increases about 4 times. In both cases this behaviour is predicted accurately by the numerical methodology.

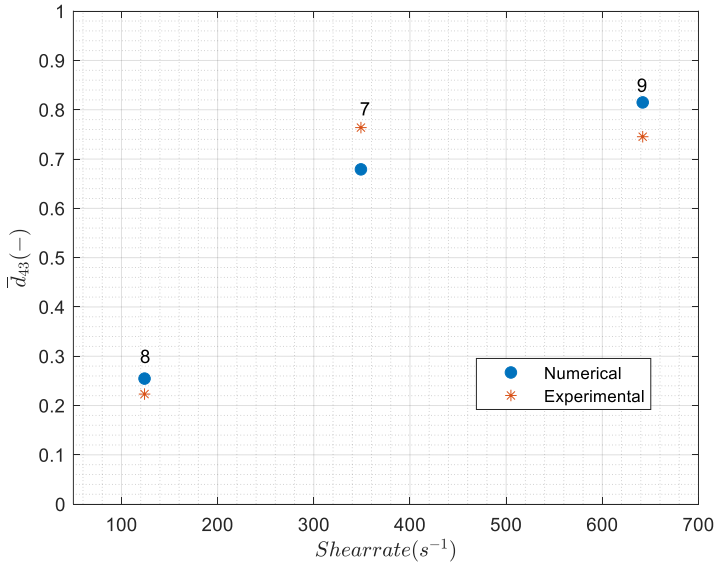

Figure 8. Numerical and experimental mean crystal size evolution over the shear rate in the case of a MSMPR including nucleation, size-independent growth and loose size-dependent agglomeration

Finally, Table 2 presents the number of iterations to solve the agglomeration PBE and the calculation time to simulate the entire converged MSMPR including nucleation, growth and agglomeration. For all the cases presented in this paper, the number of iterations remains below 70 and the calculation time is lower than 1 minute. The developed methodology is demonstrated to be efficient despite the variation of the experimental conditions.

Table 2. Numerical performances for the simulation of a continuous crystallizer including nucleation, size-independent growth and loose agglomeration.

Experiment	Number of iterations (Agglomeration PBE)	Mean total calculation time (s)
1	59	39
2	54	44
3	68	45
4	36	26
5	66	51
6	36	41
7	44	48
8	36	49
9	29	25

4. Conclusions and perspectives

In this work, a numerical methodology to solve the Population Balance Equation (PBE) including nucleation, size-independent growth and loose size-dependent agglomeration in a Mixed Suspension Mixed Product Removal (MSMPR) precipitator was developed for the steady state case. The precipitation is described by the successive resolution of two PBEs:

- The first one includes the nucleation and growth phenomena: it is solved by the numerical integration of the PBE which results in an ordinary differential equation. Its resolution leads to the crystallites size distribution and liquid phase composition.
- The second PBE considers the agglomeration of the primary particles obtained by nucleation and growth. It is solved by a discretization method and gives access to the agglomerates size distribution.

The agglomeration PBE is reformulated as a fixed point problem and its convergence is guaranteed by applying an acceleration method. The crossed-secant method manages to solve the interdependence

problem arising between the PBE and the size-dependent agglomeration kinetics. Indeed, the acceleration method leads to convergence with a zero vector as first iterate and properly describes the behaviour of the PSD in the size range going to large agglomerate sizes where the validity of the kernel expression is no more ensured.

The detailed information obtained by the numerical methodology (supersaturation, crystallites mean size, crystallization kinetics) leads to better understanding of the influence of operating conditions over the crystal size and liquid phase composition. In the future, this information can be used as a relevant input in operating conditions optimization and trouble seeking.

The results obtained by the numerical methodology were compared to a wide range of experimental data. Three operating conditions were modified: stirring rate, inlet uranium concentration and residence time. In all cases, both the accuracy of the predicted PSD and the numerical performances are independent of the operating conditions. Furthermore, the trends experimentally observed on the variations of the mean size are numerically reproduced.

Nomenclature

Latin symbols

B	Birth term	$m^{-4}\ s^{-1}$
D	Death term	$m^{-4}\ s^{-1}$
d_{43}	Volume-based mean crystal size	m
$d_{43,max}$	Maximum mean crystal size	m
$\bar{d}_{43}$	Dimensionless mean crystal size	-
F	Flowrate	$m^3\ s^{-1}$
G	Growth rate	$m\ s^{-1}$
I	Ionic strength	$mol\ m^{-3}$
K	Total quantity of nodes	-
L	Crystal size	m
L_{max}	Maximum crystal size	m
$\bar{L}$	Dimensionless crystal size	-
L^*	Nuclei size	m
M	Total quantity of streams	-
n	Number-based density function	m^{-4}
N	Total number of particles	m^{-3}
N_{max}	Maximum number of particles	m^{-3}
$\bar{N}$	Normalized number of particles	-
R	Ideal gas constant	$J\ mol^{-1}\ K^{-1}$
r_{Ag}	Agglomeration rate	$m^{-3}\ s^{-1}$
r_N	Nucleation rate	$m^{-3}\ s^{-1}$
S	Relative supersaturation	-
s	Absolute supersaturation	$mol\ m^{-3}$
T	Temperature	K
t	Time	s
t'	Agglomeration characteristic time	-

V	Reactor volume	m^3

Greek symbols

β	Agglomeration kernel	$m^3\ s^{-1}$
δ	Dirac delta function	-
$\delta_{p,q}$	Kronecker function	-
ε_a	Absolute tolerance	m^{-3}
ε'_a	Constant associated to the absolute tolerance	-
ε_r	Relative tolerance	-
η	Weight coefficient	-
μ_l	Moment of order *l*	-
$\bar{\mu}_l$	Standard moment of order *l*	-
λ	Crystal size	m
τ	Mean residence time	s
$\dot{\gamma}$	Shear rate	s^{-1}

Indices and exponents

A	Agglomeration kinetics
G	Growth kinetics
i	Stream
j	Iteration number
k	Position in the discretization vector
l	Order of moments
M	Output stream
N	Nucleation kinetics
p,q	Mother particles in agglomeration
β	Agglomeration kernel
$^-$	Dimensionless values

Abbreviations

ASD	Agglomerate size distribution
CFD	Computational Fluid Dynamics
CSD	Crystal Size Distribution
MSMPR	Mixed Solution Mixed Product Removal
PBE	Population Balance Equation
PDE	Partial Differential Equation
PSD	Particle size distribution

Acknowledgments

The authors thank ORANO for its financial support.

References

[1] A. S. Myerson, D. Erdemir, and A. Y. Lee, *Handbook of Industrial Crystallization*. Cambridge University Press, 2019. [Online]. Available: https://books.google.fr/books?id=gQVvuwEACAAJ

[2] D. Ramkrishna and M. R. Singh, “Population Balance Modeling: Current Status and Future Prospects,” *Annual Review of Chemical and Biomolecular Engineering*, vol. 5, no. 1, pp. 123–146, Jun. 2014, doi: 10.1146/annurev-chembioeng-060713-040241.

[3] T. Wang *et al.*, “Recent progress of continuous crystallization,” *Journal of industrial and engineering chemistry*, vol. 54, pp. 14–29, 2017.

[4] H. M. Omar and S. Rohani, “Crystal Population Balance Formulation and Solution Methods: A Review,” *Crystal Growth & Design*, vol. 17, no. 7, pp. 4028–4041, Jul. 2017, doi: 10.1021/acs.cgd.7b00645.

[5] L. Brivadis, V. Andrieu, É. Chabanon, É. Gagnière, N. Lebaz, and U. Serres, “New dynamical observer for a batch crystallization process based on solute concentration,” *Journal of Process Control*, vol. 87, pp. 17–26, Mar. 2020, doi: 10.1016/j.jprocont.2019.12.012.

[6] H. M. Hulburt and S. Katz, “Some problems in particle technology,” *Chemical Engineering Science*, vol. 19, no. 8, pp. 555–574, Aug. 1964, doi: 10.1016/0009-2509(64)85047-8.

[7] S. Lalleman, M. Bertrand, and E. Plasari, “Physical simulation of precipitation of radioactive element oxalates by using the harmless neodymium oxalate for studying the agglomeration phenomena,” *Journal of Crystal Growth*, vol. 342, no. 1, pp. 42–49, Mar. 2012, doi: 10.1016/j.jcrysgro.2011.01.079.

[8] C. C. Ruiz Vasquez, N. Lebaz, I. Ramière, S. Lalleman, D. Mangin, and M. Bertrand, “Fixed point convergence and acceleration for steady state population balance modelling of precipitation processes: application to neodymium oxalate,” *Chemical Engineering Research and Design*, p. S0263876221004913, Nov. 2021, doi: 10.1016/j.cherd.2021.11.030.

[9] Y. Ochi, Z. Cai, T. Horie, Y. Komoda, K.-L. Tung, and N. Ohmura, “Representative shear rate for particle agglomeration in a mixing tank,” *Chemical Engineering Research and Design*, vol. 171, pp. 73–79, Jul. 2021, doi: 10.1016/j.cherd.2021.04.017.

[10] E. D. Hollander, J. J. Derksen, O. S. L. Bruinsma, G. M. van Rosmalen, and H. E. A. van den Akker, “A Numerical Investigation into the Influence of Mixing on Orthokinetic Agglomeration,” in *10th European Conference on Mixing*, Elsevier, 2000, pp. 221–229. doi: 10.1016/B978-044450476-0/50029-7.

[11] E. D. Hollander, J. J. Derksen, O. S. L. Bruinsma, H. E. A. van den Akker, and G. M. van Rosmalen, “A numerical study on the coupling of hydrodynamics and orthokinetic agglomeration,” *Chemical Engineering Science*, vol. 56, no. 7, pp. 2531–2541, Apr. 2001, doi: 10.1016/S0009-2509(00)00435-8.

[12] D. L. Marchisio and R. O. Fox, *Computational Models for Polydisperse Particulate and Multiphase Systems*. in Cambridge Series in Chemical Engineering. Cambridge University Press, 2013. [Online]. Available: https://books.google.fr/books?id=u2EhAwAAQBAJ

[13] P. T. L. Koh, J. R. G. Andrews, and P. H. T. Uhlherr, “Modelling shear-flocculation by population balances,” *Chemical Engineering Science*, vol. 42, no. 2, pp. 353–362, 1987, doi: 10.1016/0009-2509(87)85065-0.

[14] B. V. Balakin, A. C. Hoffmann, and P. Kosinski, “Population balance model for nucleation, growth, aggregation, and breakage of hydrate particles in turbulent flow,” *AIChE J.*, p. n/a-n/a, 2009, doi: 10.1002/aic.12122.

[15] N. Lebaz, A. Cockx, M. Spérandio, and J. Morchain, “Reconstruction of a distribution from a finite number of its moments: A comparative study in the case of depolymerization process,” *Computers & Chemical Engineering*, vol. 84, pp. 326–337, Jan. 2016, doi: 10.1016/j.compchemeng.2015.09.008.

[16] L. Wang, D. L. Marchisio, R. D. Vigil, and R. O. Fox, “CFD simulation of aggregation and breakage processes in laminar Taylor–Couette flow,” *Journal of Colloid and Interface Science*, vol. 282, no. 2, pp. 380–396, Feb. 2005, doi: 10.1016/j.jcis.2004.08.127.

[17] G. Frungieri, M. U. Babler, and M. Vanni, “Shear-Induced Heteroaggregation of Oppositely Charged Colloidal Particles,” *Langmuir*, vol. 36, no. 36, pp. 10739–10749, Sep. 2020, doi: 10.1021/acs.langmuir.0c01536.

[18] G. Frungieri and M. Vanni, “Aggregation and breakup of colloidal particle aggregates in shear flow: A combined Monte Carlo - Stokesian dynamics approach,” *Powder Technology*, vol. 388, pp. 357–370, Aug. 2021, doi: 10.1016/j.powtec.2021.04.076.

[19] S. Kumar and D. Ramkrishna, “On the solution of population balance equations by discretization—I. A fixed pivot technique,” *Chemical Engineering Science*, vol. 51, no. 8, pp. 1311–1332, Apr. 1996, doi: 10.1016/0009-2509(96)88489-2.

[20] C. Brezinski, “Convergence acceleration during the 20th century,” *Journal of Computational and Applied Mathematics*, p. 21, 2000.
[21] I. Ramière and T. Helfer, “Iterative residual-based vector methods to accelerate fixed point iterations,” *Computers & Mathematics with Applications*, vol. 70, no. 9, pp. 2210–2226, Nov. 2015, doi: 10.1016/j.camwa.2015.08.025.
[22] B. Michel, T. Helfer, I. Ramière, and C. Esnoul, “A new numerical methodology for simulation of unstable crack growth in time independent brittle materials,” *Engineering Fracture Mechanics*, vol. 188, pp. 126–150, Feb. 2018, doi: 10.1016/j.engfracmech.2017.08.009.
[23] M. J. Hounslow, “A discretized population balance for continuous systems at steady state,” *AIChE Journal*, vol. 36, no. 1, pp. 106–116, Jan. 1990, doi: 10.1002/aic.690360113.
[24] M. Bertrand, E. Plasari, O. Lebaigue, P. Baron, N. Lamarque, and F. Ducros, “Hybrid LES–multizonal modelling of the uranium oxalate precipitation,” *Chemical Engineering Science*, vol. 77, pp. 95–104, Jul. 2012, doi: 10.1016/j.ces.2012.03.019.
[25] Q. Jiang and B. E. Logan, “Fractal dimensions of aggregates determined from steady-state size distributions,” *Environ. Sci. Technol.*, vol. 25, no. 12, pp. 2031–2038, Dec. 1991, doi: 10.1021/es00024a007.
[26] F. E. Kruis and K. A. Kusters, “THE COLLISION RATE OF PARTICLES IN TURBULENT FLOW,” *Chemical Engineering Communications*, vol. 158, no. 1, pp. 201–230, Apr. 1997, doi: 10.1080/00986449708936589.
[27] I. Seyssiecq, S. Veesler, D. Mangin, J. P. Klein, and R. Boistelle, “Modelling gibbsite agglomeration in a constant supersaturation crystallizer,” *Chemical Engineering Science*, vol. 55, no. 23, pp. 5565–5578, Dec. 2000, doi: 10.1016/S0009-2509(00)00185-8.
[28] A. Mersmann, *Crystallization Technology Handbook.* Hoboken: Marcel Dekker Inc., 2001.